Spectral tuning of optical coupling between air-mode nanobeam cavities and individual carbon nanotubes

H. Machiya,[1,2] T. Uda,[1,3] A. Ishii,[1,4] and Y. K. Kato[1,4,a)]
[1]*Nanoscale Quantum Photonics Laboratory, RIKEN, Saitama 351-0198, Japan*
[2]*Department of Electrical Engineering, The University of Tokyo, Tokyo 113-8656, Japan*
[3]*Department of Applied Physics, The University of Tokyo, Tokyo 113-8656, Japan*
[4]*Quantum Optoelectronics Research Team, RIKEN Center for Advanced Photonics, Saitama 351-0198, Japan*

(Received 5 October 2017; accepted 21 December 2017; published online 8 January 2018)

We demonstrate control over optical coupling between air-suspended carbon nanotubes and air-mode nanobeam cavities by spectral tuning. Taking advantage of the large dielectric screening effects caused by adsorbed molecules, laser heating is used to blueshift the nanotube photoluminescence. A significant increase in the cavity peak is observed when the nanotube emission is brought into resonance, and the spontaneous emission enhancement is estimated from the photoluminescence spectra. We find that the enhancement shows good correlation with the spectral overlap of the nanotube emission and the cavity peak. Our technique offers a convenient method for controlling the optical coupling of air-suspended nanotubes to photonic structures. https://doi.org/10.1063/1.5008299

Semiconducting carbon nanotubes (CNTs) are attractive materials for integrated photonics owing to their exceptionally small size,[1] and CNT-based discrete components such as electrically driven emitters,[2,3] photodetectors,[4,5] and single photon sources[6,7] have been demonstrated. Optical coupling to photonic structures[1,8–12] is one of the next key requirements for on-chip integration. Cavities, in particular, offer quantum electrodynamical effects for increased performance and functionality by confining electric fields into a small mode volume with a low optical loss. Exciton polaritons can form when nanotube emission is strongly coupled to a cavity,[12] whereas the interaction of CNTs with cavities results in an increased spontaneous emission rate in the weak coupling regime.[1,8–11] The spectral overlap of the emission with the cavity is an important factor in determining these effects, and the overlap can be changed by preparing samples with different cavity lengths for coupling to ensembles of CNTs.[12] Sophisticated fiber microcavities enable *in-situ* tunable coupling to individual CNTs,[6] but it still remains a challenge to perform post-fabrication tuning for on-chip cavities.

In this work, we demonstrate spectral tuning of air-suspended carbon nanotubes coupled to integrated nanobeam cavities. We utilize air-mode cavities[1,10,13] with large electric fields in air for efficient coupling to suspended CNTs. Laser heating is used to desorb molecules from the nanotubes, which offers a simple method for adjusting the nanotube emission through reduction of dielectric screening. We are able to modify the detuning by as much as 25 meV, inducing a drastic change in the cavity peak intensity. The cavity quantum electrodynamics model is used to analyze the data, and we find that the enhancement of the cavity mode can mostly be explained by the spectral overlap of the nanotube emission with the cavity peak.

The air-mode nanobeam cavities[10] [Fig. 1(f) inset] are fabricated from silicon-on-insulator wafers diced into 20-mm square chips. Electron beam lithography defines the cavity pattern, and the 260-nm-thick top silicon layer is etched through by a Bosch process in an inductively coupled plasma etcher. The 1-μm-thick buried oxide layer is then removed by 20% hydrofluoric acid, followed by another electron beam lithography process which defines the catalyst area. We finally spin-coat Fe/silica catalyst and grow CNTs onto the cavity by alcohol chemical vapor deposition at 800 °C.[14] A scanning electron microscopy image of a typical device is shown in Fig. 1(a).

The devices are measured using a room-temperature confocal microscope system.[15] An output of a wavelength-tunable Ti:sapphire laser is focused onto the sample using an objective lens with a numerical aperture of 0.8 and a working distance of 3.4 mm. We mount the sample on a motorized three-dimensional feedback stage, which allows for efficient automated measurements. Photoluminescence (PL) is collected using the same objective lens and detected using a liquid-nitrogen-cooled InGaAs diode array attached to a spectrometer. Laser reflection comes back through the objective lens and is detected with a Si photodiode, which is used to align to the cavity position. Samples are placed in nitrogen to avoid oxidation of nanotubes at high excitation powers.

The cavities are designed to have resonances near the emission energy of chiralities with large population to maximize the probability of coupling, and more than 10 000 cavities are prepared on a chip. Nanotubes optically coupled to the cavity are located by one-dimensional PL scans over the nanobeams. The automated scan results are filtered by performing peak detection and linewidth estimation. Since the cavity linewidth is considerably narrower than the nanotube linewidth at room temperature, devices showing a sharp peak component are chosen for detailed characterization.

A typical PL spectrum of a single CNT coupled to a cavity is shown in Fig. 1(b) where the excitation laser power

a)Author to whom correspondence should be addressed: yuichiro.kato@riken.jp

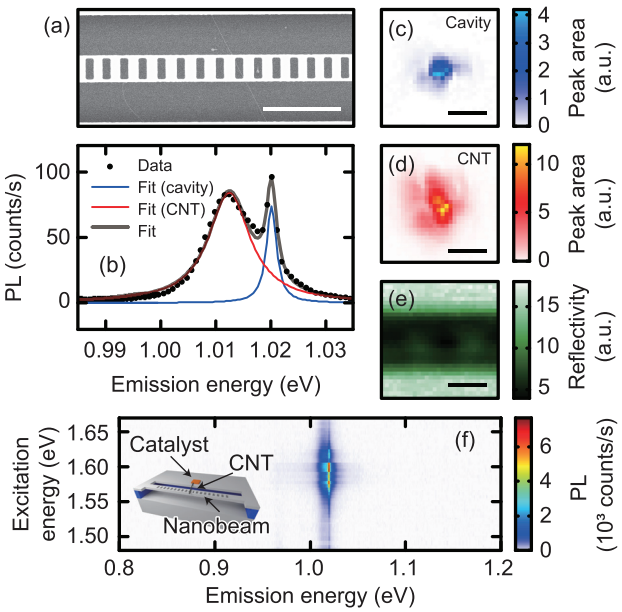

FIG. 1. (a) Scanning electron microscopy image of a fabricated cavity with an air-suspended CNT. The scale bar is 2 μm. (b) Typical PL spectrum of a cavity coupled to a CNT. Black dots are data and solid lines are the Lorentzian multi-peak fits. $P = 1\,\mu$W and an excitation laser energy of 1.594 eV are used. (c) and (d) Spectrally resolved PL images of the cavity emission and the nanotube PL, respectively. PL spectra are fitted to two Lorentzian functions with fixed center energies and linewidths corresponding to the cavity and the CNT peaks. The peak areas are used to construct the images. (e) Reflectivity image taken simultaneously with (c) and (d). For (c)–(e), $P = 200\,\mu$W and an excitation energy of 1.590 eV are used, and the scale bars are 2 μm. (f) PL excitation map of the device taken with $P = 50\,\mu$W. The inset is a schematic of a device. In (b) and (f), spectra are taken where the cavity emission is maximized. For all PL measurements, laser polarization is perpendicular to the nanobeam.

$P = 1\,\mu$W is used. We use two Lorentzian functions to decompose the spectrum into the sharp cavity mode (blue) and the broad nanotube emission (red), and spectrally resolved PL images [Figs. 1(c) and 1(d)] are obtained by spatially mapping each peak area. Combined with the reflectivity image [Fig. 1(e)], we find that the sharp component is localized at the center of the device [Fig. 1(c)], consistent with the spatial extent of the cavity mode. In comparison, the spectrally broad component is distributed across the width of the trench [Fig. 1(d)], showing the location and the length of the CNT. To confirm that the CNT is individual, the PL excitation map is also taken [Fig. 1(f)]. A single peak in the map confirms that the cavity is coupled to an individual CNT, and its chirality is assigned to be (10,5) by comparing to tabulated data.[15]

Looking at Fig. 1(b), the nanotube emission needs blueshifting by ~10 meV to achieve resonance. In order to tune the optical transition energy, we take advantage of the sensitivity of air-suspended nanotubes to dielectric screening. By controlling the amount of adsorbed molecules through temperature or pressure, large spectral shifts of up to 30 meV have been observed.[16–19] We utilize laser heating to induce molecular desorption in our devices, which is a simple and convenient method. As the excitation power is increased, the nanotube peak blueshifts due to molecular desorption while the cavity peak gradually brightens [Fig. 2(a)]. The nanotube emission is brought into resonance at $P \sim 200\,\mu$W, enhancing cavity emission intensity. By further increasing the excitation power, the cavity peak becomes weaker again as the nanotube peak continues to blueshift. Above $P \sim 250\,\mu$W, we do not find additional blueshifting because the molecules are fully desorbed.

In Fig. 2(b), we compare on- and off-resonance spectra, which are indicated by orange and green curves, respectively. We find an enhancement of the cavity peak height by a factor of 10 at resonance, while the nanotube peak height remains comparable due to the increased non-radiative recombination rate at high powers.[15] The significant difference in the cavity peak height indicates that the optical coupling to the nanotube emission is modified by the spectral shift. The spectral lineshape of the nanotube peak is changed at high powers (green curve), probably due to the inhomogeneous molecular desorption.

To quantitatively characterize the spectral tuning effect, the excitation power dependence is analyzed by decomposing the spectra into the cavity and the nanotube peak components. We first fit the sharp cavity peak to a single Lorentzian function using a fitting window of ~10 meV, yielding the cavity peak energy $\hbar\omega_{\mathrm{cav}}$, linewidth γ, and peak area I_{cav}. Due to the complex nanotube lineshape, we let the nanotube peak spectrum $L_{\mathrm{CNT}}(\omega)$ to be the fitting residual, where ω is the frequency. The nanotube peak area I_{CNT} is defined as the integral $I_{\mathrm{CNT}} = \int L_{\mathrm{CNT}}(\omega)\mathrm{d}\omega$, while the peak energy $\hbar\omega_{\mathrm{CNT}}$ is defined as the weighted average $\hbar\omega_{\mathrm{CNT}} = \hbar\frac{\int \omega L_{\mathrm{CNT}}(\omega)\mathrm{d}\omega}{\int L_{\mathrm{CNT}}(\omega)\mathrm{d}\omega}$.

In Fig. 2(c), we plot the peak energies as a function of the excitation power, and blueshifting of the nanotube peak by as much as 18 meV (red open circles) is observed. A slight redshift of the cavity peak (blue dots) likely originates from the heating-induced increase of the refractive index.[20] The energy shifts of the nanotube and cavity together allow for energy

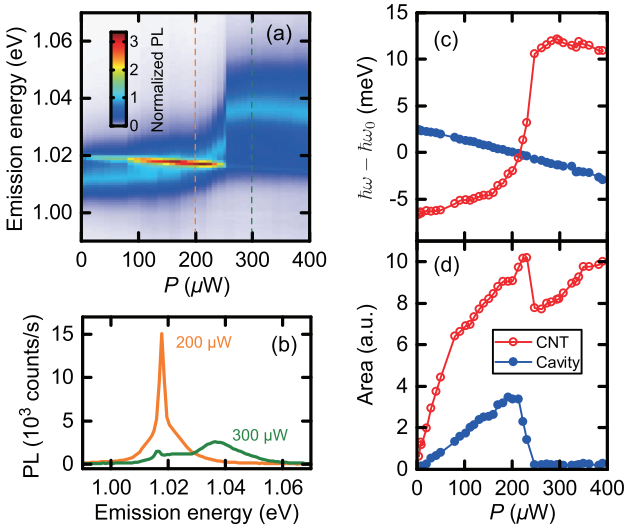

FIG. 2. (a) Excitation power dependence of PL. PL is normalized with respect to the nanotube peak height. Vertical dashed lines indicate the powers where PL spectra in (b) are taken. (b) Comparison of PL spectra taken at $P = 200\,\mu$W (orange) and 300 μW (green). (c) and (d) Excitation power dependence of the peak center energy and peak area, respectively. Red open circles are obtained from the CNT peak, and the blue dots are taken from the cavity emission. The peak center energies are plotted as the difference from the resonant energy $\hbar\omega_0 = 1.018$ eV. For (a)–(d), excitation laser energy is tuned to E_{22} resonance and laser polarization is perpendicular to the nanobeam.

detuning $\hbar\omega_{cav} - \hbar\omega_{CNT}$ to be changed from +9 meV to −14 meV. The tuning range is sufficiently large for modulating the optical coupling of the nanotubes to the cavity, as it considerably exceeds the nanotube emission linewidth at room temperature. We note that the shifts are reversible upon reduction of the excitation power (supplementary figure in the supplementary material).

We now turn our attention to the excitation power dependence of emission intensities [Fig. 2(d)]. I_{CNT} increases linearly at low excitation powers and then becomes sublinear as a result of the exciton-exciton annihilation process,[15] with a drastic drop at $P = 250\,\mu$W [Fig. 2(d), red open circles]. Since the E_{22} resonance also blueshifts by molecular desorption,[17–19] the sudden drop can be understood by the shifting of the E_{22} resonance away from the excitation energy. In comparison, we observe a linear increase of I_{cav} with excitation power, for the region below $P = 190\,\mu$W [Fig. 2(d), blue dots]. The sublinearity of I_{CNT} is likely cancelled out by the improvement of coupling, because the nanotube peak approaches resonance in this power region. The cavity peak area then rapidly reduces above $P = 200\,\mu$W as a result of the increased energy detuning.

Since we are changing the excitation power, we need to characterize the optical coupling by evaluating emission enhancement. Assuming that stimulated emission is negligible, the spontaneous emission enhancement factor is given by $F = \frac{I_{cav}/\eta_{cav}}{I_{CNT}/\eta_{CNT}}$, where η_{CNT} and η_{cav} are the collection efficiencies of the nanotube and the cavity emission, respectively. To obtain conservative estimates of F, $\eta_{CNT}/\eta_{cav} = 0.49$ is used.[10]

We have calculated F using the data shown in Fig. 2, and the results are plotted in Fig. 3(a). As the excitation power is increased up to $P = 190\,\mu$W, the enhancement factor increases from 0.056 to 0.19, and F rapidly decreases by a factor of 15 at $P = 250\,\mu$W. The large modification to the enhancement factor is consistent with the spectral shifts in this range. Above $P = 250\,\mu$W, we do not observe much excitation power dependence.

The enhancement factor is known to be determined by the spectral overlap, spatial overlap, and polarization matching.[21,22] If we assume that the nanotube does not move during our experiment, F should only depend on the spectral overlap. As the nanotube lineshape is complex, we need to evaluate the spectral overlap without assuming a particular emitter lineshape. We first consider a simple case of a monochromatic emitter coupled to a cavity with a Lorentzian lineshape. The spontaneous emission enhancement at a frequency ω is then given by

$$\frac{3}{4\pi^2}\left(\frac{\lambda_0^3}{V}\right)\left(\frac{\omega}{\gamma}\right)\frac{(\gamma/2)^2}{(\omega-\omega_{cav})^2+(\gamma/2)^2}, \tag{1}$$

where λ_0 and V are the wavelength and the mode volume of the cavity, respectively.[23] We multiply the cavity enhancement and the normalized lineshape of the nanotube emission and integrate over the full spectrum to obtain

$$F = \frac{3}{4\pi^2}\left(\frac{\lambda_0^3}{V}\right)S, \tag{2}$$

where the integral

$$S = \int\left(\frac{\omega}{\gamma}\right)\frac{(\gamma/2)^2}{(\omega-\omega_{cav})^2+(\gamma/2)^2}\frac{L_{CNT}(\omega)}{I_{CNT}}\,d\omega \tag{3}$$

is the generalized form of the spectral overlap. $1/S$ reduces to $1/Q_{cav} + 1/Q_{CNT}$ under an assumption that the nanotube lineshape is a Lorentzian resonant with the cavity,[23] where Q_{cav} and Q_{CNT} are the quality factors of the cavity and the nanotube peaks, respectively. If Q_{cav} is considerably larger than Q_{CNT}, the upper bound of S would be given by Q_{CNT}.

The spectral overlap can be calculated for arbitrary lineshapes using Eq. (3), and the results of numerical integration are plotted in Fig. 3(b). When the excitation power is increased, we observe a crossover from a gradual increase to a rapid decrease at $P = 190\,\mu$W as the nanotube peak shifts through the cavity peak. The maximum spectral overlap $S = 73$ is reasonable, considering that $Q_{CNT} \sim 80$.

Correlation between the enhancement factor and the spectral overlap is examined in Fig. 3(c). Indeed, F increases monotonically with S as expected from Eq. (2). We note that the detuning changes sign above and below $P = 190\,\mu$W, but similar enhancements are obtained for red- (open circles) and blue-detuned (crosses) nanotube emission. It is reasonable that detuning sign does not have an effect, because F should only depend on S.

In Fig. 4, we present two additional devices that have different initial detunings. In the second device, the nanotube peak is initially resonant with the cavity at the lowest excitation power [Fig. 4(a)]. When the excitation power is increased, molecular desorption shifts the nanotube peak away from the cavity, reducing the enhancement [Fig. 4(b)]. The blueshifting results in the spectral overlap to decrease as well [Fig. 4(c)], explaining the behavior of F. The third device has an initial detuning even larger than the first device [Fig. 4(d)]. Even for the fully desorbed state, there exists considerable emission enhancement [Fig. 4(e)]. The spectral overlap increases with the excitation power but shows a less pronounced increase at the resonance compared to F [Fig. 4(f)]. The peak values of F are comparable to the average enhancement previously reported.[10]

Figures 4(g) and 4(h) are the F–S plots of the second and third devices, respectively. We observe a monotonic increase of F as observed in the first device, consistent with

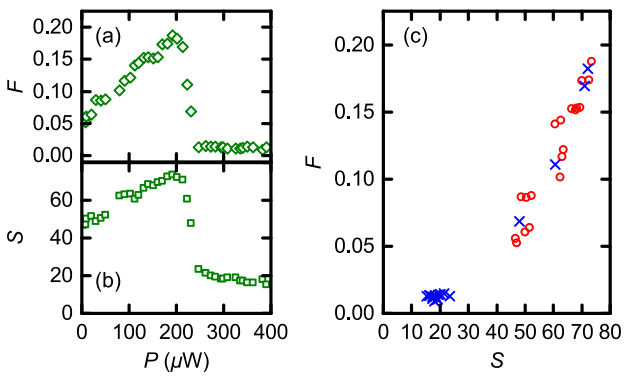

FIG. 3. (a) and (b) Excitation power dependence of F and S, respectively. F and S are calculated from the results in Fig. 2. (c) F as a function of S. Open circles indicate red-detuned nanotube emission ($P \leq 190\,\mu$W) and crosses correspond to blue-detuned conditions ($P > 190\,\mu$W).

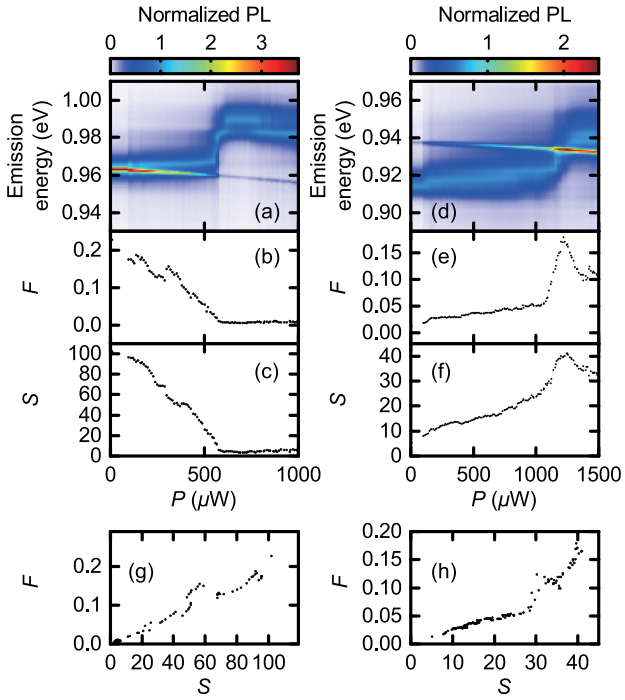

FIG. 4. (a) Normalized PL, (b) F, and (c) S as a function of excitation power for the second device. (d) Normalized PL, (e) F, and (f) S as a function of excitation power for the third device. (g) and (h) S dependence of F for the second and third devices, respectively. Excitation laser energy and polarization are tuned to maximize the signal.

the understanding that the enhancement factor is determined by the spectral overlap. It is interesting to note that the slope of the F–S plot should be $\frac{3}{4\pi^2}\frac{\lambda_0^3}{V} = 3.2$ for perfect spatial and polarization overlaps.[10] The linear fits to our experimental data, in comparison, yield slopes on the order of 10^{-3}, which suggests that there remains a lot of room for improving the coupling. Better spatial and polarization alignment could be possible by site-controlled transfer of nanotubes or photonic crystal structures by micromanipulation.[24,25] We also note that the experimental slope may be an underestimate because of our conservative calculation of F. The actual F is expected to be higher since the collection efficiency of the nanotube emission should be enhanced due to the photonic crystal structure.[10,21]

It is intriguing that we observe a slight superlinearity in the F–S plots for the first and third devices [Figs. 3(c) and 4(h)]. One possible explanation is the cavity-resonant optical forces. We assume in our analysis that the spatial overlap does not change during our measurements, but the overlap may improve at resonance if the CNTs are pulled towards the electric field maximum.[26,27] Another possibility is stimulated emission which contributes to additional emission into the cavity mode. In the first and third devices, the spectral overlap becomes larger at high excitation powers, which is preferable for stimulated emission. The second device, in comparison, has a smaller spectral overlap at high powers, which may explain why the superlinearity cannot be observed. By controlling the pressure or temperature, it should be possible to keep the resonant condition and perform excitation power dependence measurements as well as photon correlation measurements[28] to identify the contribution from stimulated emission.

In summary, spectral tuning of air-suspended carbon nanotubes coupled to air-mode nanobeam cavities is demonstrated by laser-heating-induced molecular desorption. We have performed excitation power dependence measurements and have shown that such molecular-scale effects provide a convenient *in-situ* method for controlling the coupling of as-grown CNTs to photonic structures. The excitation power dependence is characterized using the enhancement factor, and we find that the numerically calculated spectral overlap can explain the behavior. The tunability of optical coupling would be a key not only for fundamental understanding of the light-matter interaction in CNTs but also for reconfigurable optical devices in the telecom band on a silicon platform.

See supplementary material for the down-sweep excitation power dependence.

We thank S. Chiashi and S. Maruyama for the use of the electron microscope. This work was supported by JSPS (KAKENHI JP16H05962 and JP16K13613) and MEXT (Photon Frontier Network Program, Nanotechnology Platform). The samples were fabricated at the Center for Nano Lithography & Analysis at The University of Tokyo. H.M. was supported by RIKEN Junior Research Associate Program, and T.U. was supported by ALPS and JSPS Research Fellowship.

[1]F. Pyatkov, V. Fütterling, S. Khasminskaya, B. S. Flavel, F. Hennrich, M. M. Kappes, R. Krupke, and W. H. P. Pernice, "Cavity-enhanced light emission from electrically driven carbon nanotubes," Nat. Photonics **10**, 420 (2016).
[2]T. Mueller, M. Kinoshita, M. Steiner, V. Perebeinos, A. A. Bol, D. B. Farmer, and P. Avouris, "Efficient narrow-band light emission from a single carbon nanotube p–n diode," Nat. Nanotechnol. **5**, 27 (2010).
[3]N. Higashide, M. Yoshida, T. Uda, A. Ishii, and Y. K. Kato, "Cold exciton electroluminescence from air-suspended carbon nanotube split-gate devices," Appl. Phys. Lett. **110**, 191101 (2017).
[4]J. U. Lee, "Photovoltaic effect in ideal carbon nanotube diodes," Appl. Phys. Lett. **87**, 073101 (2005).
[5]Y. Kumamoto, M. Yoshida, A. Ishii, A. Yokoyama, T. Shimada, and Y. K. Kato, "Spontaneous exciton dissociation in carbon nanotubes," Phys. Rev. Lett. **112**, 117401 (2014).
[6]A. Jeantet, Y. Chassagneux, C. Raynaud, P. Roussignol, J. S. Lauret, B. Besga, J. Estève, J. Reichel, and C. Voisin, "Widely tunable single-photon source from a carbon nanotube in the Purcell regime," Phys. Rev. Lett. **116**, 247402 (2016).
[7]A. Ishii, T. Uda, and Y. K. Kato, "Room-temperature single-photon emission from micrometer-long air-suspended carbon nanotubes," Phys. Rev. Appl. **8**, 054039 (2017).
[8]R. Watahiki, T. Shimada, P. Zhao, S. Chiashi, S. Iwamoto, Y. Arakawa, S. Maruyama, and Y. K. Kato, "Enhancement of carbon nanotube photoluminescence by photonic crystal nanocavities," Appl. Phys. Lett. **101**, 141124 (2012).
[9]S. Imamura, R. Watahiki, R. Miura, T. Shimada, and Y. K. Kato, "Optical control of individual carbon nanotube light emitters by spectral double resonance in silicon microdisk resonators," Appl. Phys. Lett. **102**, 161102 (2013).
[10]R. Miura, S. Imamura, R. Ohta, A. Ishii, X. Liu, T. Shimada, S. Iwamoto, Y. Arakawa, and Y. K. Kato, "Ultralow mode-volume photonic crystal nanobeam cavities for high-efficiency coupling to individual carbon nanotube emitters," Nat. Commun. **5**, 5580 (2014).
[11]A. Noury, X. L. Roux, L. Vivien, and N. Izard, "Enhanced light emission from carbon nanotubes integrated in silicon micro-resonator," Nanotechnology **26**, 345201 (2015).
[12]A. Graf, L. Tropf, Y. Zakharko, J. Zaumseil, and M. C. Gather, "Near-infrared exciton-polaritons in strongly coupled single-walled carbon nanotube microcavities," Nat. Commun. **7**, 13078 (2016).
[13]F. Liang and Q. Quan, "Detecting single gold nanoparticles (1.8 nm) with ultrahigh-Q air-mode photonic crystal nanobeam cavities," ACS Photonics **2**, 1692 (2015).

[14]S. Maruyama, R. Kojima, Y. Miyauchi, S. Chiashi, and M. Kohno, "Low-temperature synthesis of high-purity single-walled carbon nanotubes from alcohol," Chem. Phys. Lett. **360**, 229 (2002).
[15]A. Ishii, M. Yoshida, and Y. K. Kato, "Exciton diffusion, end quenching, and exciton-exciton annihilation in individual air-suspended carbon nanotubes," Phys. Rev. B **91**, 125427 (2015).
[16]P. Finnie, Y. Homma, and J. Lefebvre, "Band-gap shift transition in the photoluminescence of single-walled carbon nanotubes," Phys. Rev. Lett. **94**, 247401 (2005).
[17]J. Lefebvre and P. Finnie, "Excited excitonic states in single-walled carbon nanotubes," Nano Lett. **8**, 1890 (2008).
[18]Y. Homma, S. Chiashi, T. Yamamoto, K. Kono, D. Matsumoto, J. Shitaba, and S. Sato, "Photoluminescence measurements and molecular dynamics simulations of water adsorption on the hydrophobic surface of a carbon nanotube in water vapor," Phys. Rev. Lett. **110**, 157402 (2013).
[19]T. Uda, A. Ishii, and Y. K. Kato, "Single carbon nanotubes as ultrasmall all-optical memories," ACS Photonics (published online 2017).
[20]M. El Kurdi, X. Checoury, S. David, T. P. Ngo, N. Zerounian, P. Boucaud, O. Kermarrec, Y. Campidelli, and D. Bensahel, "Quality factor of Si-based photonic crystal L3 nanocavities probed with an internal source," Opt. Express **16**, 8780 (2008).
[21]S. Noda, M. Fujita, and T. Asano, "Spontaneous-emission control by photonic crystals and nanocavities," Nat. Photonics **1**, 449 (2007).
[22]D. C. Unitt, A. J. Bennett, P. Atkinson, D. A. Ritchie, and A. J. Shields, "Polarization control of quantum dot single-photon sources via a dipole-dependent Purcell effect," Phys. Rev. B **72**, 033318 (2005).
[23]M. P. van Exter, G. Nienhuis, and J. P. Woerdman, "Two simple expressions for the spontaneous emission factor β," Phys. Rev. A **54**, 3553 (1996).
[24]C. C. Wu, C. H. Liu, and Z. Zhong, "One-step direct transfer of pristine single-walled carbon nanotubes for functional nanoelectronics," Nano Lett. **10**, 1032 (2010).
[25]T. Tajiri, S. Takahashi, Y. Ota, J. Tatebayashi, S. Iwamoto, and Y. Arakawa, "Demonstration of a three-dimensional photonic crystal nanocavity in a ⟨110⟩-layered diamond structure," Appl. Phys. Lett. **107**, 071102 (2015).
[26]H. Ajiki, T. Iida, T. Ishikawa, S. Uryu, and H. Ishihara, "Size- and orientation-selective optical manipulation of single-walled carbon nanotubes: A theoretical study," Phys. Rev. B **80**, 115437 (2009).
[27]S. Mandal, X. Serey, and D. Erickson, "Nanomanipulation using silicon photonic crystal resonators," Nano Lett. **10**, 99 (2010).
[28]Y. Ota, M. Kakuda, K. Watanabe, S. Iwamoto, and Y. Arakawa, "Thresholdless quantum dot nanolaser," Opt. Express **25**, 19981 (2017).